

# Active Flow Control Strategy of Laminar Separation Bubbles Developed over Subsonic Airfoils at Low Reynolds Numbers

Justin Aholt\* and Fathi Finaish†

*Missouri University of Science & Technology, Rolla, MO, 65401*

A computational parametric study designed to examine the plausibility of an external body force generated by active means, such as a plasma actuator, as a way of controlling a Laminar Separation Bubble (LSB) over an airfoil at low Reynolds numbers was conducted. Computational Fluid Dynamics (CFD) was employed to characterize the effect that a body force, localized to a small region tangent to the airfoil surface, might have on an LSB. In this study, the effects of altering the strength and location of the “actuator” on the size and location of the LSB and on the aerodynamic performance of the airfoil were observed. It was found that the body force, when properly located and with sufficient magnitude, could effectively eliminate the LSB. Additionally, it was found that by eliminating the LSB, the aerodynamic efficiency of the airfoil could be improved by as much as 60%. Thus, it was determined that such a system may indeed be an effective measure of reducing or eliminating the negative effects associated with LSBs at low Reynolds numbers, making the strategy an excellent candidate for future experimental research regarding this topic.

## Nomenclature

$\alpha$	Airfoil angle of attack (deg)
$\rho_\infty$	Free-stream density (kg/m <sup>3</sup> )
$a_\infty$	Free-stream speed of sound (m/s)
$c$	Airfoil chord (m)
$C_p$	Pressure Coefficient = $\frac{p-p_\infty}{1/2\rho_\infty V_\infty^2}$
$f_d$	Force magnitude per unit volume (N/m <sup>3</sup> )
$f_{nd}$	Dimensionless force per unit volume = $\frac{f_d c}{\rho_\infty V_\infty^2}$
$M_\infty$	Free-stream Mach number = $\frac{V_\infty}{a_\infty}$
$Re$	Reynolds number = $\frac{\rho_\infty V_\infty c}{\mu}$
$V_\infty$	Free-stream velocity (m/s)
$x$	Chord-wise position with respect to airfoil leading edge ( $c$ )
$X_s$	Chord-wise position with respect to nominal LSB separation point ( $c$ )
$y$	Position with respect to airfoil chord (normal to $x$ )

## I. Introduction

LAMINAR Separation Bubbles (LSBs) have been encountered in many subsonic, low Reynolds number aerospace applications, including turbo-machinery, high altitude UAVs, and wind turbines. As described by Ramesh,<sup>1</sup> an LSB is a phenomenon which occurs when a laminar boundary layer encounters an adverse pressure gradient, detaches, undergoes a turbulent transition, and reattaches downstream, resulting in the flow structure shown in figure 1. LSBs are widely regarded as parasitic because they typically have the

\*Graduate Research Assistant, Department of Mechanical and Aerospace Engineering, 1870 Miner Circle, Rolla, MO, Student Member AIAA

†Professor, Department of Mechanical and Aerospace Engineering, Associate Fellow, AIAA

effect of increasing drag, thus reducing aerodynamic efficiency.<sup>2</sup> Additionally, LSBs are characteristically sensitive to small fluctuations in upstream flow characteristics, and are consequently prone to instability.<sup>3-5</sup> This instability results in design uncertainty, and has been experimentally observed to reduce aerodynamic performance as well as result in potentially dangerous dynamic structural loading in aerospace structures.<sup>5,6</sup> Consequently, methods of controlling or eliminating LSBs are a priority of many aerodynamicists. The most effective methods of LSB elimination currently in use involve forcing premature turbulent transition of the boundary layer, making it less likely to separate; e.g. careful airfoil selection or the placement of mechanical turbulators upstream of the laminar separation point.<sup>3,5</sup> However, such methods are typically passive, generating turbulence regardless of necessity. In applications where a system must perform under a wide range of operating conditions (such as a UAV or wind turbine), an active control system is desirable. It is for this reason that flow control systems such as pneumatic turbulators and plasma actuators are of current research interest.<sup>7</sup> Plasma actuators have been identified as a potential practical means of applying the control strategy outlined in this paper.

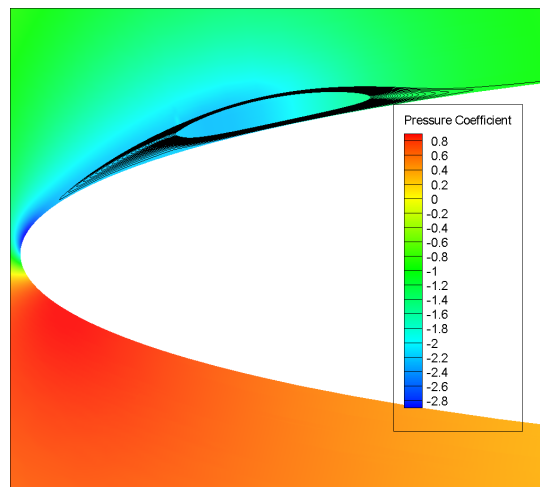


Figure 1. Stream traces and pressure coefficient contour plot of an LSB ( $Re = 10^5$ ,  $f_{nd} = 0$ )

An aerodynamic plasma actuator is a relatively simple device, consisting of a pair of electrodes: one exposed to the surrounding atmosphere, and one embedded within a dielectric material, arranged in an asymmetric configuration,<sup>8</sup> as shown in figure 2. A radio frequency ac voltage on the order of 1-10 kV is applied across the electrodes, inducing a Dielectric Barrier Discharge (DBD), a phenomenon resulting in the generation of a weakly ionized, low temperature plasma near the exposed electrode.<sup>8-10</sup> This discharge has the effect of imparting momentum into the fluid near the actuator, the effect of which can be modeled as a localized body force. The DBD is unique among plasma discharges, in that it is sustainable under atmospheric conditions, and thus well suited to conventional aerodynamic applications.<sup>8</sup> DBD inducing plasma actuators have found a wide variety of aerodynamic applications, including flow separation prevention over low Reynolds number airfoils and turbine blades,<sup>11,12</sup> high Mach number flow control,<sup>13</sup> and vortex generation.<sup>14</sup> The successful implementation of DBDs in a number of low Reynolds number applications suggests that they may be suitable as a means of controlling other low Reynolds number phenomena, such as LSBs.

Many different approaches have been made to modeling DBDs, ranging in complexity from a rudimentary potential flow analysis<sup>15</sup> to full-scale integration of the Maxwell and Navier-Stokes equations.<sup>10,14,16,17</sup> As reported by Enloe *et al.*,<sup>8</sup> a DBD plasma is highly structured, but necessarily unsteady with respect to time, discharging and terminating regularly as a function of the applied voltage amplitude and waveform. However, the timescale on which this process occurs is typically small ( $<1$  ms under atmospheric conditions) compared with the characteristic fluid timescales. Hence, for many aerodynamic applications, a plasma actuator may be adequately modeled as a time-steady localized body force.<sup>9,17</sup> In this study, an existing CFD code was modified to incorporate such a force.

In contrast to the previously mentioned LSB elimination strategies, a plasma actuator or similar body force generation system would hypothetically eliminate LSBs by injecting enough momentum into the bound-

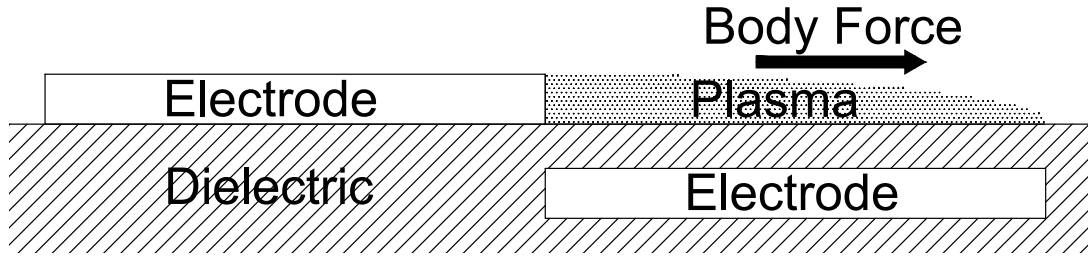


Figure 2. Potential approach of external force generation: Plasma actuator (cross-section)

ary layer to overcome the adverse pressure gradient responsible for flow separation. There are several advantages that a plasma actuator, if successfully implemented, could offer over competing LSB elimination technologies. A plasma actuator can be actively controlled, with significantly lower response times than are possible via mechanical systems. Thus, a plasma actuator could be designed to respond to varying flow-field conditions, or powered off when unneeded. Additionally, as a solid state system, a plasma actuator requires no moving parts, potentially reducing system weight requirements and maintenance costs. The potential that a plasma actuator represents as a flow control system is the motivation for this research.

In this study, a 16 percent thick elliptical airfoil at a 10 degree angle of attack and a chord Reynolds number of  $10^5$  was selected as a standard condition upon which to test the effect of various body force locations and magnitudes. The control condition in this study was the case in which no body force was applied ( $f_{nd} = 0$ ). This case has been confirmed by several numerical studies<sup>2,18</sup> to produce a stable LSB near the leading edge of the airfoil, making it an ideal test case for this study. Under this condition, the LSB has been shown to have a separation point  $0.0107 c$  and reattachment point  $0.1850 c$  downstream of the airfoil leading edge (in the chord-wise direction). The airfoil's lift and drag coefficients were found to be 0.8484 and 0.0528, respectively, corresponding to a lift to drag ratio of approximately 16.1. The flow-field about the leading edge of the airfoil in the control case is shown in figure 1. The location and strength of the applied body force were varied to determine the optimal conditions under which the actuator would perform.

## II. Computational Approach

It was immediately evident that the most economical way to deal with the complexity of the outlined problem was through Computational Fluid Dynamics (CFD). For this study, the structured grid Reynolds-Averaged Navier-Stokes approach was applied. This method allows for relatively high quality local grid generation, which in turn yields accurate results. To assure quality results, the applied analysis process required scrutiny in two areas: grid generation and flow solving.

### II.A. Grid Generation

Grid control was a particular area of interest in this study. Because actuator location was a variable in this study, it was necessary to modify the grid used in the prior study,<sup>2</sup> in order to assure that the volume to which the body force was applied did not vary with the location of of the force-applied region. It was found that solution stability was highly sensitive to the grid intensity near the leading edge of the LSB. This can be explained by the principle that if a grid is not sufficiently defined within areas of high pressure or velocity gradients, the flow solver can not be expected to converge on an accurate or numerically stable solution.<sup>19</sup> Unfortunately, the flow solver used could not handle more than a set number of surface grid points. After an extensive validation study, a suitable grid was obtained, which consistently produced results that were accurate with respect to the previously mentioned studies.<sup>2,18</sup> The surface grid used contains the flow-solver imposed limit of 250 points, with greater point density in the areas of highest airfoil curvature, and in the region of interest around the LSB.

## II.B. Flow Field Solution Methodology

In this study, the time-steady Navier-Stokes equations were applied to solve the given flow-field. The flow solver used in this study was OVERFLOW, a 3-dimensional, time-accurate, Reynolds-Averaged Navier-Stokes (RANS) flow solver, originally developed by NASA to simulate flow over the Space Shuttle, but later modified to handle more conventional flight conditions.<sup>20</sup> It has a demonstrated ability to produce accurate results for low-speed subsonic flow conditions and has been used in the design process of many aircraft. OVERFLOW was selected in this case both for its fidelity and its mutability; the source code of this software was readily available to these authors. The turbulence model selected for this study was the one-equation Spalart-Allmaras (SA) model, both for being relatively economical, and for its capability to accurately predict free-shear flow.

As previously mentioned, OVERFLOW was selected due to its ability to be modified. This feature was necessary, because of the requirement to locally apply a body force. An additional body force source term was incorporated into the OVERFLOW source code. A new variable was defined, here denoted  $f_{nd}$ , defined as

$$f_{nd} = \frac{f_d c}{\rho_\infty V_\infty^2}. \quad (1)$$

## II.C. Input Parameters

The only flow parameters specified in this study were the angle of attack ( $\alpha$ ), free-stream Mach number ( $M_\infty$ ), and chord Reynolds number ( $Re$ ). For this study,  $\alpha$  was set at 10 degrees,  $M_\infty$  at 0.01, and  $Re$  at  $10^5$ . For comparative purposes, under standard atmospheric conditions, this corresponds to a free-stream velocity of 3.43 m/s and a chord-length of 0.43 m. The applied body force was oriented in the chord-wise direction for all cases. The region over which the body force was applied over the airfoil was  $0.02 c$  along the airfoil surface and  $0.003 c$  in height, corresponding to 8.9 mm and 1.3 mm for the given Reynolds and Mach numbers, and assuming standard sea level conditions for air. The maximum magnitude of the body force was selected conservatively, such that the actuator produced a peak velocity increase of roughly 2 m/s for the stated assumptions. This acceleration has been far exceeded in laboratory settings,<sup>21</sup> and should be readily attainable in practice.

## III. Results and Discussion

To better represent the obtained results, a new coordinate system is defined. The location of the leading edge of the actuator is used as the X-axis variable in the following analysis, as indicated in figure 3. As shown,  $X_s$  is defined as the location of the leading edge of the actuator with respect to the laminar separation point of the control case. This schematic also shows the direction of the applied body force.

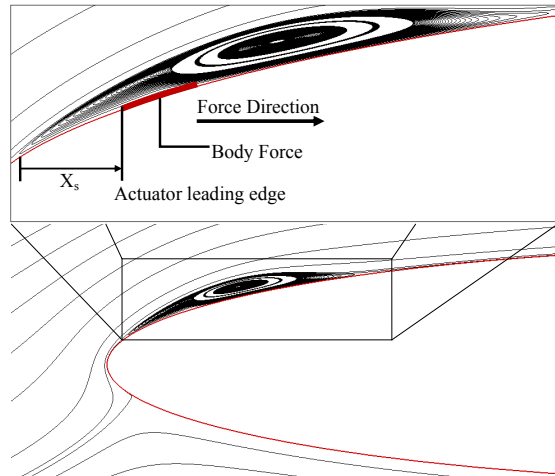
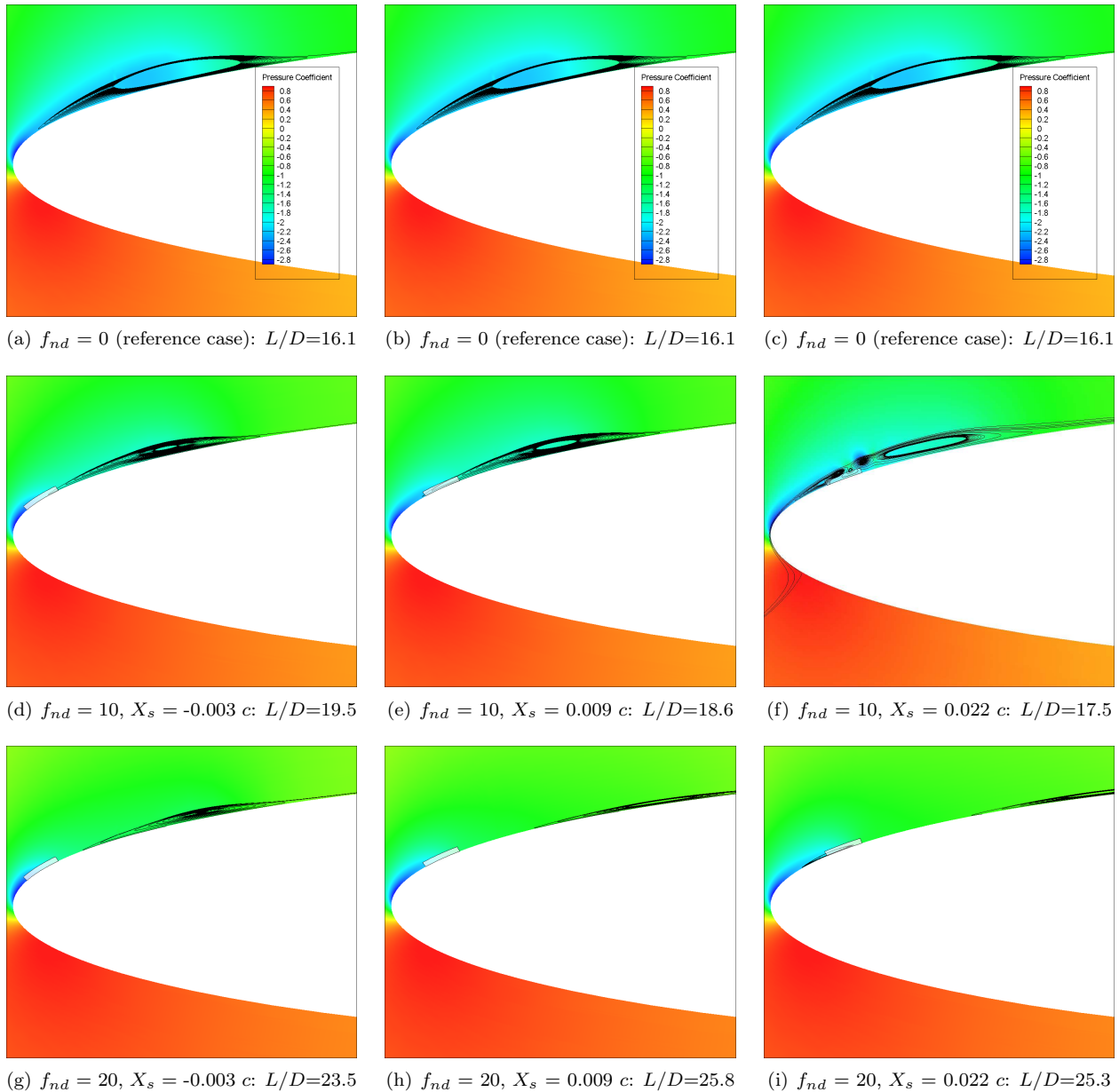


Figure 3. Coordinate system used in analysis

Figure 4 shows the effect of the body force magnitude and location on the LSB and airfoil lift to drag ratio. This figure is organized into three rows. The top row shows the reference case, where no actuator was applied. The center and bottom rows show the effects of actuator placement on LSB development for actuator strengths  $f_{nd} = 10$  and  $20$ , respectively. In subfigures d through i, the actuator location is indicated with a pale highlight.



**Figure 4. Influence of actuator strength and location on LSB development and corresponding airfoil lift to drag ratio**

As shown, when placed upstream of the nominal separation point ( $X_s = -0.003$ ), the actuator has the effect of shrinking the LSB in all dimensions. As the actuator is moved  $0.009 c$  downstream of the separation point, the same effect is observed, but to a lesser effect in the  $f_{nd} = 10$  case. In the  $f_{nd} = 20$  case, the LSB appears to have been simultaneously “squeezed” to the airfoil surface and “stretched” laterally. The laminar separation point is clearly shifted downstream from the nominal location. As observed for  $f_{nd} = 10$ , as the actuator is moved further downstream to  $X_s = 0.022 c$ , it causes additional flow complexity in the form of an LSB breakup. As shown in figure 4.f, two smaller clockwise rotating bubbles are clearly visible upstream of the primary one, which interact to induce secondary counter-clockwise rotation. Here, the effective airfoil shape does not appear to have been significantly altered with respect to that of the reference case. As

shown in figure 4.i, for  $f_{nd} = 20$ , as the actuator is shifted to  $X_s = 0.022 c$ , the LSB is merely shifted and stretched further downstream. However, a secondary separation point has formed upstream of the actuator, near the nominal separation point. From this information, it would appear that moving the actuator too far downstream of the laminar separation point results in the reformation of the LSB upstream of the actuator. Figure 4 also shows a correlation between LSB size reduction and airfoil aerodynamic performance. As indicated, the cases in which the LSB size is reduced most tend to yield higher lift-to-drag ratios than their counterparts. This correlation is discussed in greater detail in sections III.A and III.B.

Figures 5 through 7 give the computed pressure coefficient distribution of the airfoil over the upper leading edge of the airfoil for various force magnitudes at given actuator locations. Each figure contains two plots: one conventionally plotting the pressure coefficient against  $X_s$ , and a second plotting  $C_p$  against  $y$ . The  $C_p$  vs.  $y$  plots are relevant to this analysis because they can be integrated to find the net pressure drag over the airfoil, just as  $C_p$  vs  $x$  plots can be integrated to determine lift. The location of the LSB in each case roughly corresponds to the location of the secondary suction peak located downstream of the airfoil’s natural peak. The reason that LSBs tend to reduce aerodynamic efficiency is their tendency to degrade the natural suction peak of the airfoil. The most significant consequence of this increase in pressure over the leading edge of the airfoil is a dramatic increases in pressure drag. In extreme cases, it can also reduce the lift generated by the airfoil.<sup>2</sup> It follows, then, that airfoil performance can be enhanced by restoring the “natural” suction peak of the airfoil. As shown in figures 5 through 7, regardless of actuator location, as the magnitude of the body force is increased, the primary suction peak of the airfoil becomes more pronounced. This is the physical mechanism responsible for the improvement in the aerodynamic efficiency of the airfoil. The greatest improvement is shown in figure 6, with an  $f_{nd}$  of 20. As shown, in this case the suction peak associated with the LSB has effectively vanished, and the natural suction peak has been restored. Not coincidentally, this case corresponded to the greatest improvements seen in the lift-to-drag ratio of the airfoil. Of special note in figure 7 is the existance of multiple distinct pressure peaks for all but one of the cases. This is the result of the LSB breakup previously mentioned, wherein multiple distinct bubbles are observed.

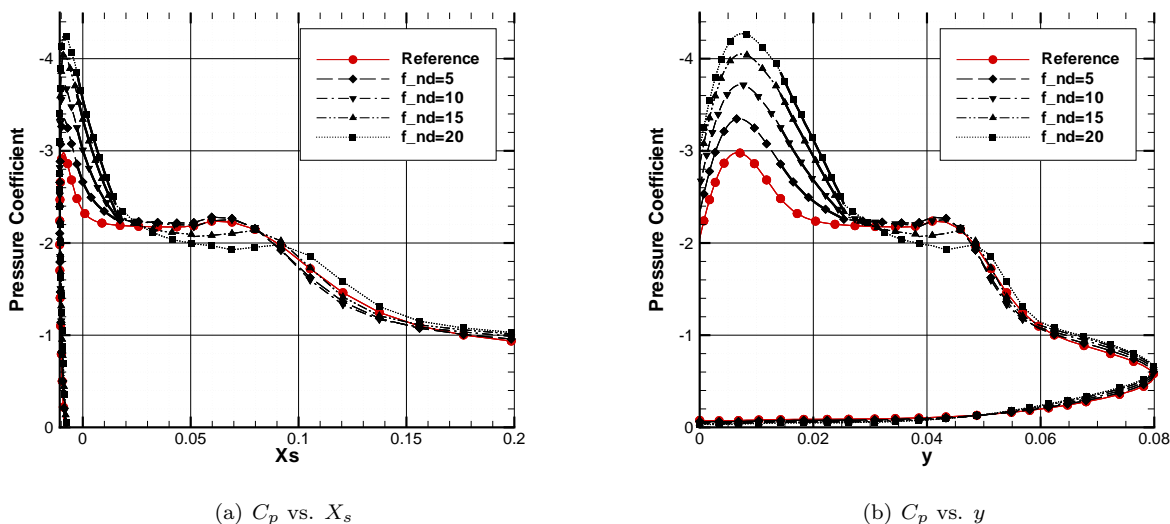
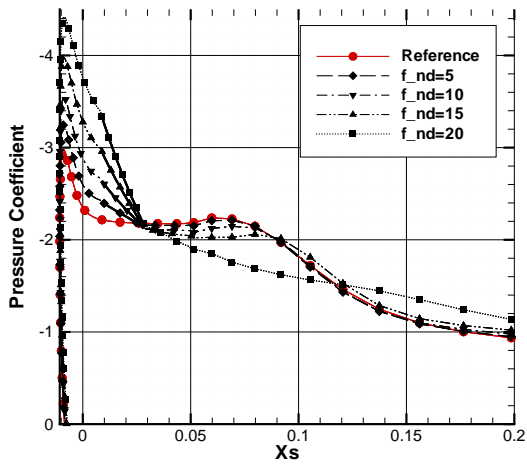


Figure 5. Influence of actuator strength on pressure distribution over upper leading edge of airfoil ( $X_s = -0.003 c$ )

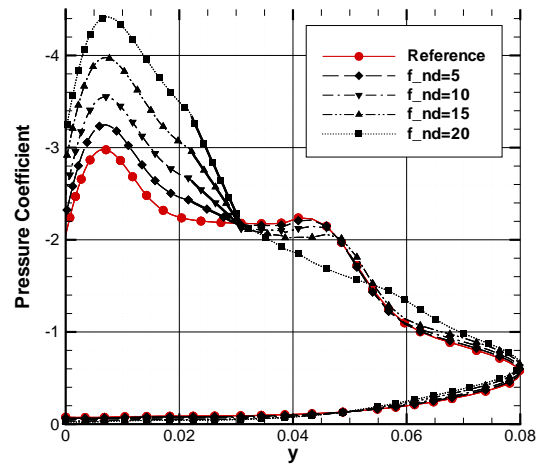
For convenience, figures 8 and 9 are provided, complementing the data shown in figures 5 through 7. Figures 8 and 9 show the effect of moving the actuator downstream for two force magnitudes. As shown, the optimal location of the actuator with respect to pressure peak restoration is dependant upon force magnitude. This is consistent with the observations previously made with respect to the LSB size and airfoil lift to drag ratio.

### III.A. Dependence of LSB size on actuator strength and position

In order to quantitatively examine the relationship between the actuator strength/position and the size of the bubble, and thus the change in the effective airfoil shape, a new parameter was defined. The comparative

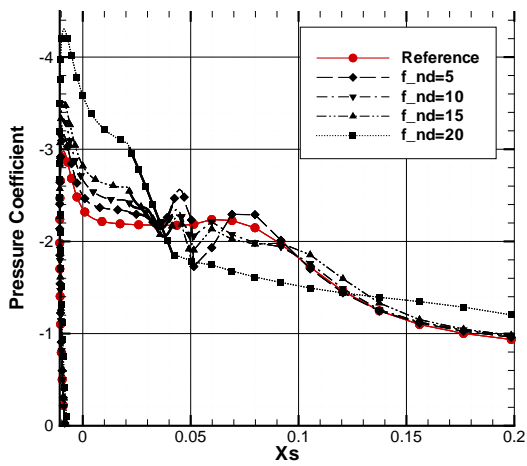


(a)  $C_p$  vs.  $X_s$

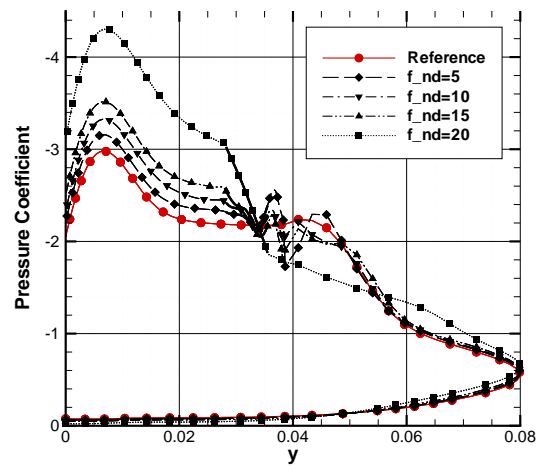


(b)  $C_p$  vs.  $y$

Figure 6. Influence of actuator strength on pressure distribution over upper leading edge of airfoil ( $X_s = 0.009 c$ )

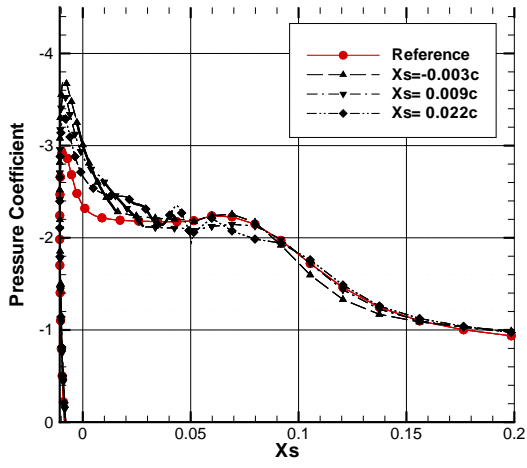


(a)  $C_p$  vs.  $X_s$

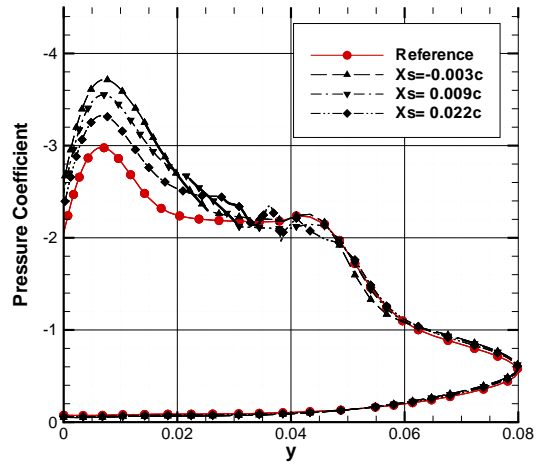


(b)  $C_p$  vs.  $y$

Figure 7. Influence of actuator strength on pressure distribution over upper leading edge of airfoil ( $X_s = 0.022 c$ )

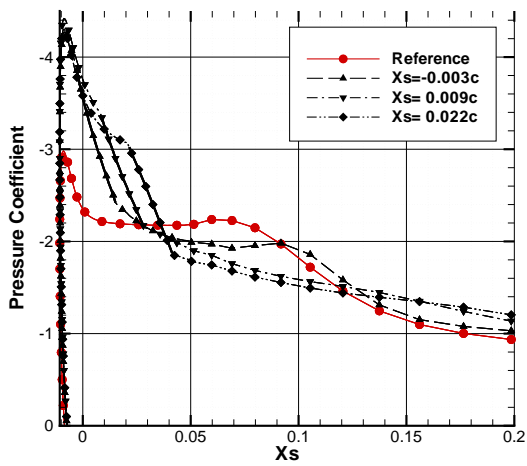


(a)  $C_p$  vs.  $X_s$

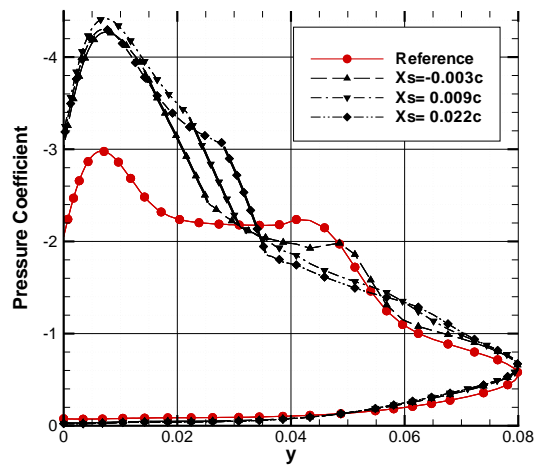


(b)  $C_p$  vs.  $y$

Figure 8. Influence of actuator location on pressure distribution over upper leading edge of airfoil ( $f_{nd} = 10$ )



(a)  $C_p$  vs.  $X_s$



(b)  $C_p$  vs.  $y$

Figure 9. Influence of actuator location on pressure distribution over upper leading edge of airfoil ( $f_{nd} = 20$ )

area plotted in figure 10 is simply the product of the chord-wise length of the bubble and the height of the center of rotation with respect to the airfoil surface. It is merely a means of comparing solutions, and should not be treated as a direct measure of the area of the LSB. Figure 10 shows the dependence of the comparative area of the LSB on actuator position, for  $f_{nd}$  magnitudes of 0, 5, 10, 15, and 20.

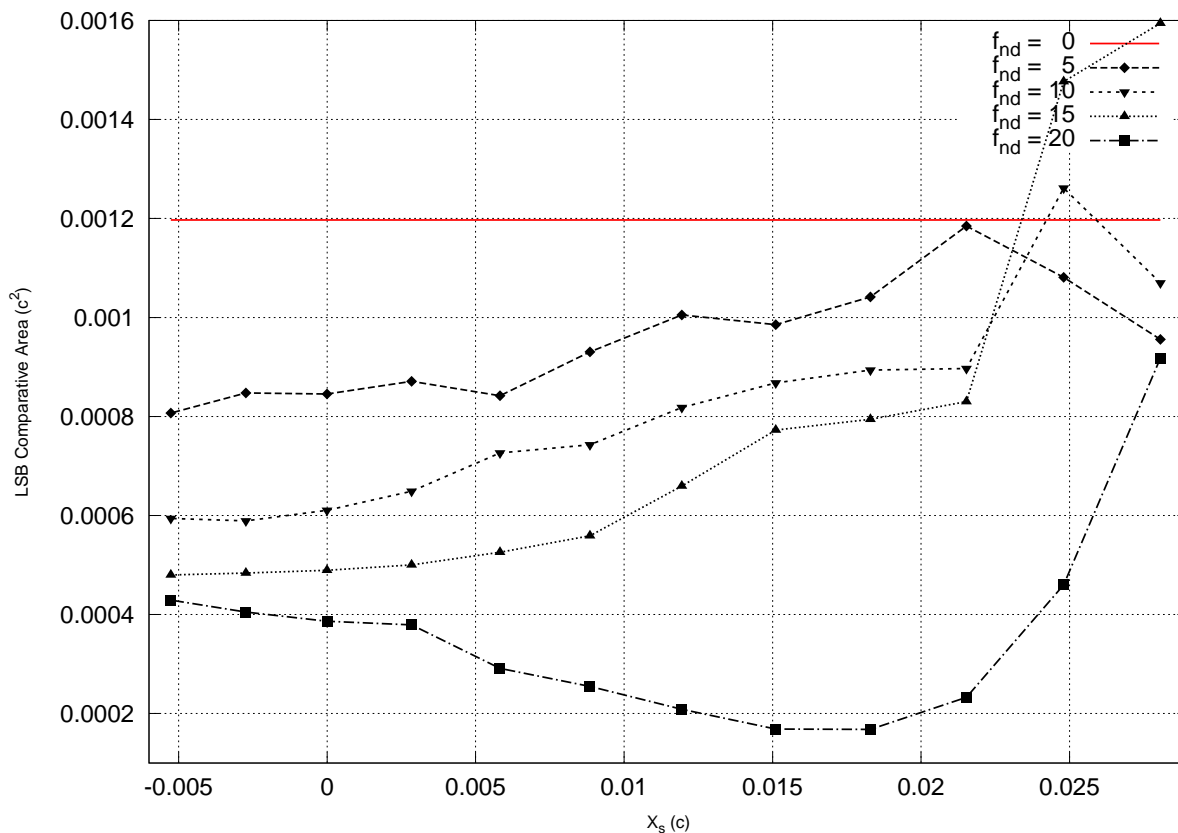


Figure 10. Influence of actuator location and strength on LSB size

As shown in figure 10, it was found that increasing the body force magnitude generally reduced the size of the LSB. This is in agreement with intuition, as a body force applied in the direction of the fluid motion would be expected to counteract the adverse pressure gradient responsible for the initial flow separation. It was found that for  $f_{nd}$ s of 5, 10, and 15, the location of the actuator which resulted in minimum LSB size was upstream of the nominal leading edge of the LSB. For each of these cases, optimal actuator performance was observed to occur when the actuator was “straddling” the LSB separation point, with the actuator leading edge upstream of the separation point, and the trailing edge downstream. However, for an  $f_{nd}$  of 20, the optimal actuator location was found to be roughly 0.017  $c$  downstream of the LSB separation point. This discrepancy was unexpected. It may be the case that the larger force magnitude had a strong enough upstream influence to achieve the desirous effect seen in the other cases, and that downstream placement had a greater effect on the rest of the bubble. However, more research is required to confirm this hypothesis. It may also be the case that the discrepancy was the result of error associated with the crudeness of the method to determine LSB area. However this suggestion would seem to be partially discredited by the airfoil performance data given in section III.B. The trends described in this section break down as the actuator leading edge is moved roughly 0.2  $c$  downstream of the LSB separation point for the  $f_{nd} = 5, 10,$  and 15 cases, as shown in figure 10. This phenomenon is the result of actuator-induced flow-field complexity, more fully discussed in section III.C.

### III.B. Dependence of airfoil aerodynamic performance on actuator strength and position

Figure 11 gives the lift to drag ratio of the airfoil versus actuator location for various force magnitudes. As shown, the actuator location corresponding to peak aerodynamic efficiency is not constant with respect to  $f_{nd}$ . For  $f_{nd} = 5$  and 10, the optimal actuator leading edge location is slightly upstream of the nominal LSB leading edge. For the  $f_{nd} = 15$  case, optimal efficiency occurs when the actuator is placed 0.005  $c$  downstream of the separation point, and for the  $f_{nd} = 20$  case, this occurs at approximately 0.013  $c$ . It was found that for an  $f_{nd}$  of 5, the lift to drag ratio of the airfoil could be improved by 8.1 percent at  $X_s = -0.0027 c$  (0.0027  $c$  upstream of the separation point). For an  $f_{nd}$  of 10, the lift to drag ratio could be increased by 21.8 percent at  $X_s = 0$ . At  $f_{nd} = 15$ , the lift to drag ratio could be improved by 39.8 percent at  $X_s = 0.0028 c$ . At  $f_{nd} = 20$ , the lift to drag ratio was found to improve by 61.2 percent to 25.9 at  $X_s = 0.0119 c$ .

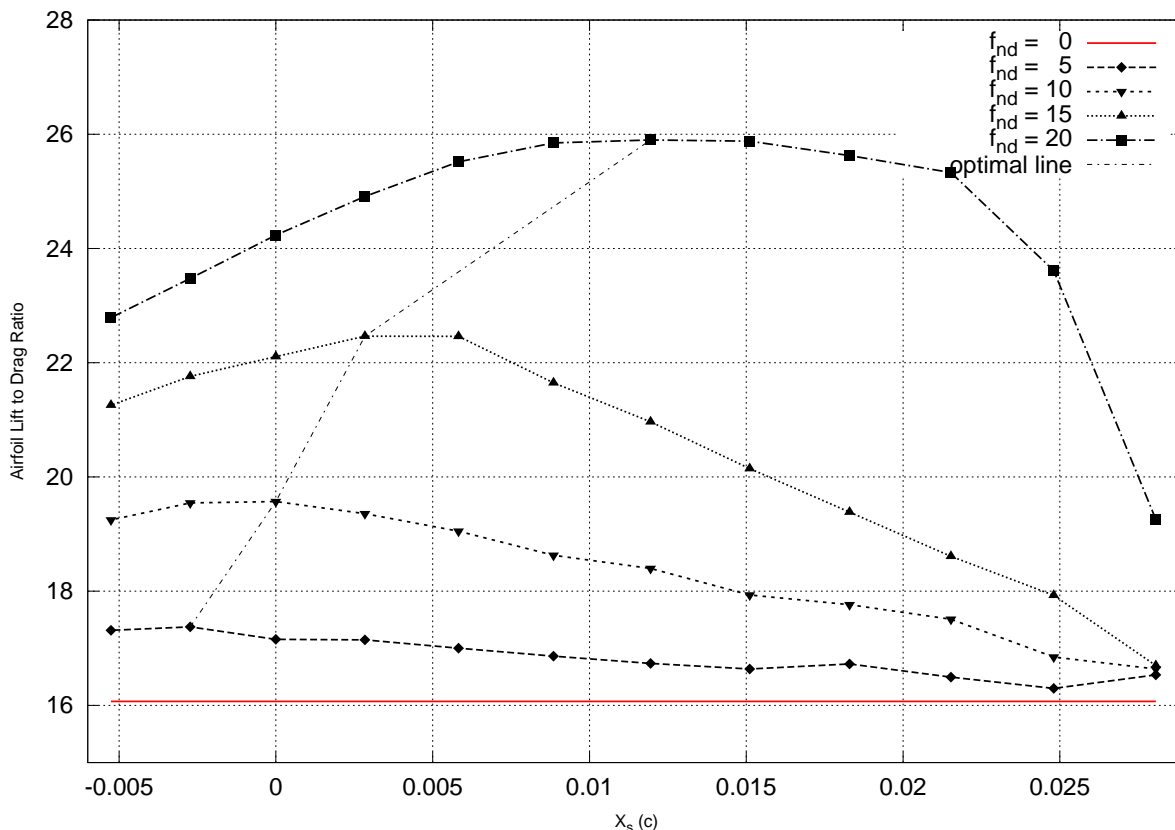


Figure 11. Dependence of Airfoil Lift to Drag Ratio on actuator strength and location

Although the optimal locations of the actuator with respect to the LSB area and airfoil efficiency are not identical, it is apparent from the data that the shrinking or elimination of the LSB generally corresponds to improvements in aerodynamic efficiency. Comparing the case whereby the maximum performance enhancement was attained to the reference case, this trend becomes apparent. Under the maximum performance case, the actuator effectively eliminates the LSB, as shown in figure 12, which compares that case to the control case.

The lift and drag coefficients obtained from this solution were 0.9591 and 0.0370, corresponding to a lift to drag ratio of 25.90. By comparison, in the reference case, the airfoil had a lift coefficient of 0.8486, a drag coefficient of 0.0528, and a lift to drag ratio of 16.08. The actuator had the effect of increasing the lift of the airfoil by 13 percent over the nominal case, and reducing the drag by 30 percent, improving the lift to drag ratio by 61 percent. Presumably, this boost in lift can be explained by the actuator induced acceleration of the flow over the upper surface of the airfoil. The drag reduction can be explained by the restoration of the leading edge suction peak of the airfoil, as previously established.

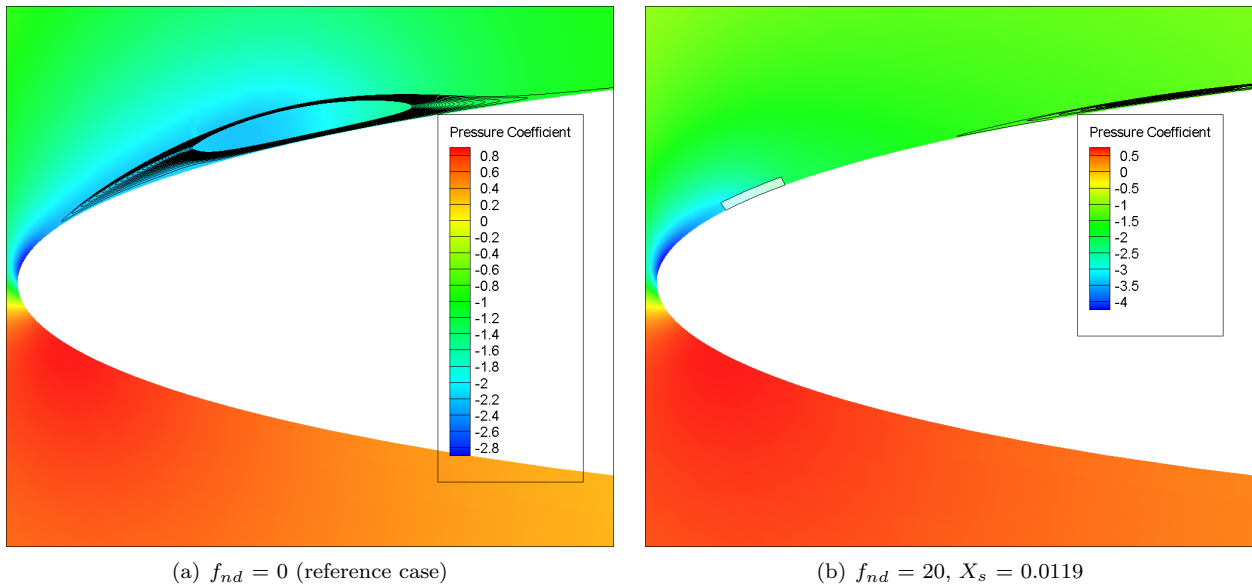


Figure 12. Comparison between stream traces and pressure coefficient contour plots for control case and optimal performance case

As a second actuator performance barometer, a high Reynolds number case, under which an LSB is not observed can be examined. Here, a case identical to the control case, but with a Reynolds number of 2 million is observed. The lift coefficient, drag coefficient, and lift-to-drag ratio of this case are computed to be 0.7530, 0.0256, and 29.44, respectively. As figure 13 shows, the actuator has the effect of restoring the pressure distribution over the leading edge of the airfoil to something roughly similar to that attained at a Reynolds number of 2 million without an actuator. In fact, the leading edge suction peak of the optimized case is superior to that observed at higher Reynolds numbers. Compared with the high Reynolds number case, the optimal solution featured 27 percent greater lift, and 45 percent greater drag (compared with the 106 percent increase in drag associated with reference case). The lift to drag ratio was merely 12 percent lower than that attained at a Reynolds number of 2 million. The actuator has the effect of marginally increasing the lift of the airfoil (already inflated due to the low Reynolds number), while drastically reducing the drag associated with the LSB.

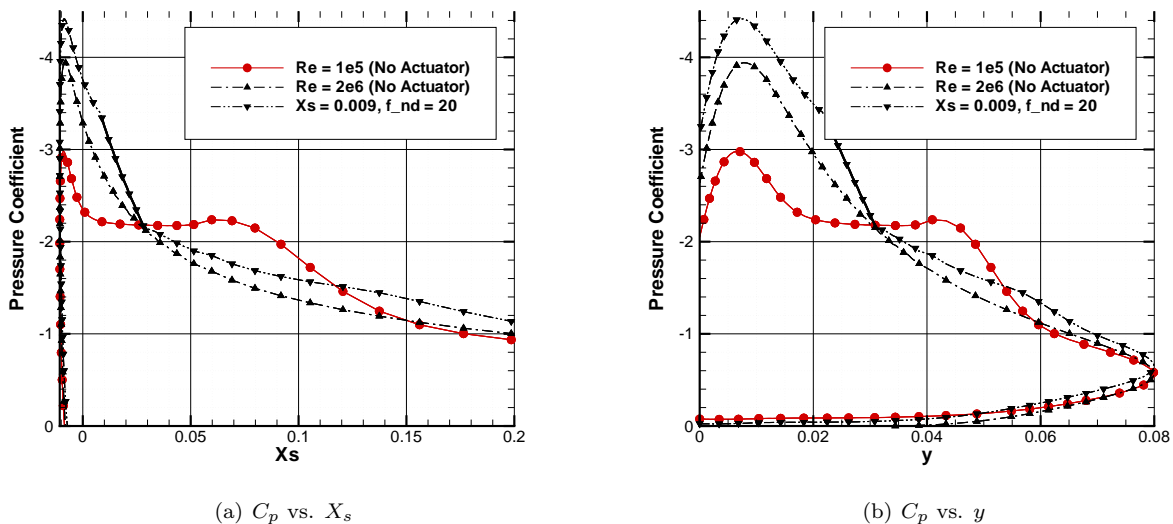


Figure 13. Comparison between Pressure Distributions of optimal performance case and control case with Reynolds number of 2 million

### III.C. Observation of actuator induced LSB breakup and instability

As previously mentioned, erratic LSB behavior is observed as the actuator is moved significantly downstream of the laminar separation point. This appears to be the result of an LSB breakup induced by the actuator. As shown in figure 14, as the actuator is progressively shifted downstream of the nominal separation point, additional clockwise circulatory regions appear upstream of the primary LSB core. These separate circulations ultimately interact, inducing secondary counter-rotational flow between them. This behavior results in progressively increasing flow-field complexity, rendering the applied method of measuring LSB size inadequate, and ultimately resulting in flow-field instability. This behavior was noted in each of the  $X_s = 5, 10,$  and  $15$  cases. As suggested, the stability of the LSB is highly sensitive to the location of the actuator, when located downstream of the laminar separation point.

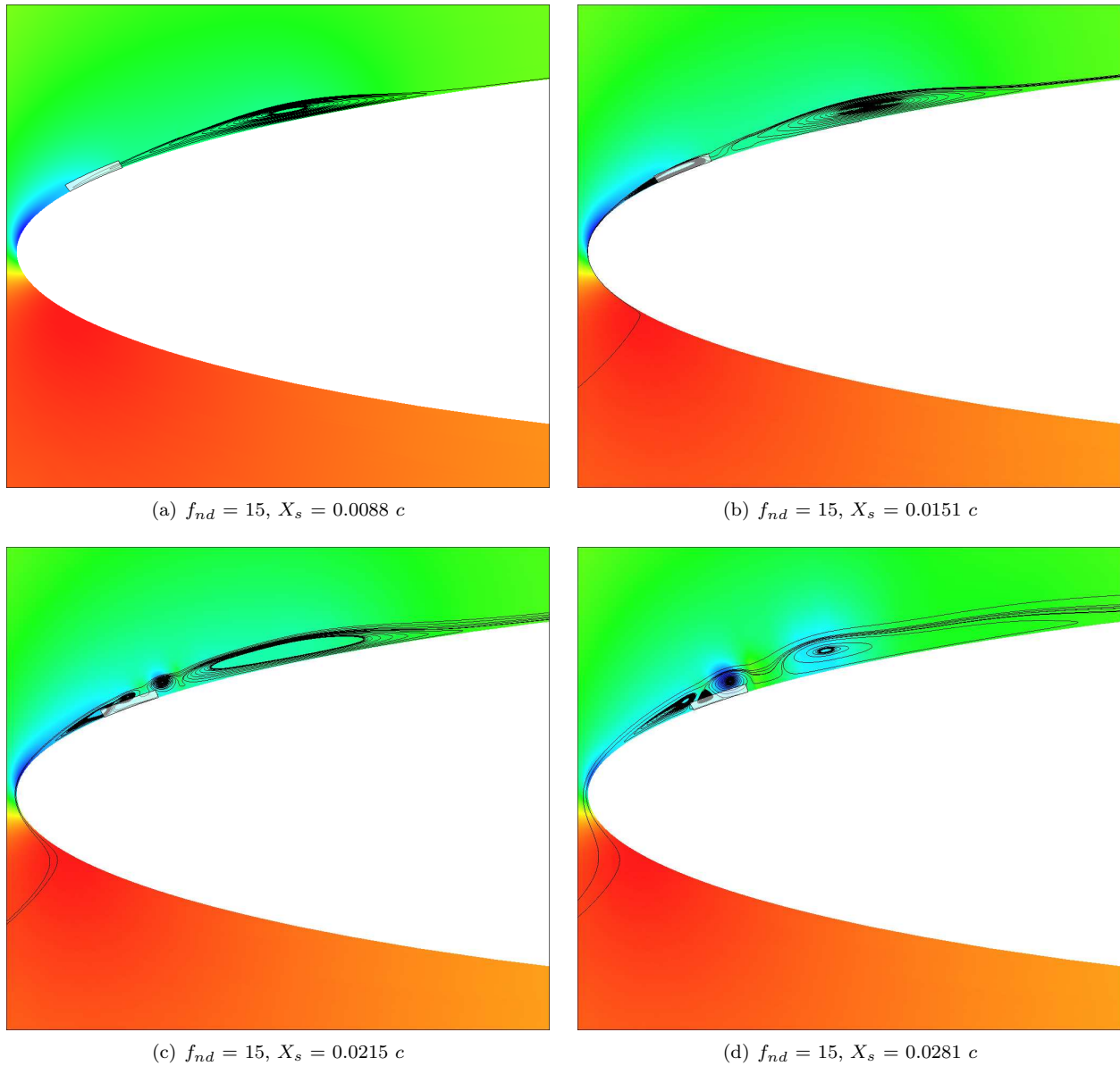


Figure 14. Evolution of LSB structure as actuator is shifted downstream of nominal separation point

## IV. Conclusions

A body force generation system, such as a plasma actuator, would appear to make an ideal low Reynolds number aerodynamic performance enhancement device, particularly in the presence of LSBs. In this study, it was found that a localized body force was capable of significantly reducing the size of an LSB, or even eliminating it entirely. The actuator was found to marginally increase lift, while dramatically reducing the drag associated with the LSB. The resultant aerodynamic efficiency of the airfoil was comparable to that attained by the same airfoil at high Reynolds numbers, where the LSB was not observed. These results, given the relatively conservative modeling of the actuator, are encouraging. With a larger body force magnitude, or lower characteristic Reynolds numbers, the application of an external body force might result in aerodynamic performance surpassing that found at very high Reynolds numbers. However, the effect the actuator had on both the size of the LSB and the aerodynamic performance of the airfoil was highly sensitive to the physical placement of the actuator. It was found that the optimal location of the actuator with respect to the LSB varied with the actuator's strength, but that it was always near the nominal separation point. If placed too far downstream of the separation point, the actuator was found to induce flow instability. Despite this, the results of this study are promising for body force generation systems, such as plasma actuators, as a means of eliminating LSBs and generally improving low Reynolds number aerodynamic performance. This study warrants further experimental research into the feasibility of plasma actuators in such applications.

## Acknowledgements

The authors gratefully acknowledge the facilities and resources provided by the Missouri University of Science and Technology. This work was supported by the the NASA Missouri Space Grant Consortium (MOSGC).

## References

- <sup>1</sup>Ramesh, O. N. and Diwan, S. S., "Laminar Separation Bubbles: Dynamics and Control," *Sadhana - Academy Proceedings in Engineering Sciences*, Indian Academy of Sciences, Bangalore, India, 2007, pp. 1–7.
- <sup>2</sup>Aholt, J., "Influence of Laminar Separation Bubbles on the Aerodynamic Characteristics of Elliptical Airfoils at Low Reynolds Numbers," *2008-2009 Missouri Space Grant Consortium Student Reports and Abstracts*, MOSGC, Columbia, MO, April 2009.
- <sup>3</sup>Rist, U. and Augustin, K., "Control of Laminar Separation Bubbles Using Instability Waves," *AIAA Journal*, Vol. 44, No. 10, 2006, pp. 2217–2223.
- <sup>4</sup>Zaman, K. and McKinzie, D. J., "Control of "Laminar Separation" Over Airfoils by Acoustic Excitation," *27th AIAA Aerospace Sciences Meeting and Exhibit*, AIAA, Ren, NV, Jan. 1989.
- <sup>5</sup>Bak, C., Madsen, H. A., Fuglsang, P., and Rasmussen, F., "Observations and Hypothesis of Double Stall," *Wind Energy*, Vol. 2, No. 1, 1999, pp. 195–210.
- <sup>6</sup>Schreck, S. J. and Robinson, M. C., "Horizontal Axis Wind Turbine Blade Aerodynamics in Experiments and Modeling," *IEEE Transactions on Energy Conversion*, Vol. 22, No. 1, 2007, pp. 61–70.
- <sup>7</sup>Horstmann, K., Quast, A., and Boermann, L., "Pneumatic turbulators - a device for drag reduction at Reynolds numbers below 5 106," Agard-cp-365, AGARD, 1984.
- <sup>8</sup>Enloe, C. L., McLaughlin, T. E., VanDyken, R. D., Kachner, K. D., Jumper, E. J., and Corke, T. C., "Mechanisms and Responses of a Single Dielectric Barrier Plasma Actuator: Plasma Morphology," *AIAA Journal*, Vol. 42, No. 3, 2004, pp. 589–593.
- <sup>9</sup>Shyy, W., Jayaraman, B., and Andersson, A., "Modeling of glow discharge-induced fluid dynamics," *Journal of Applied Physics*, Vol. 92, No. 11, 2002, pp. 6434–6443.
- <sup>10</sup>Orlov, D. M. and Corke, T. C., "Numerical Simulation of Aerodynamic Plasma Actuator Effects," *43rd AIAA Aerospace Sciences Meeting and Exhibit*, AIAA, Ren, NV, Jan. 2005.
- <sup>11</sup>Sosa, R. and Artana, G., "Steady control of laminar separation over airfoils with plasma sheet actuators," *Journal of Electrostatics*, Vol. 64, 2006, pp. 604–610.
- <sup>12</sup>Huang, J., Corke, T. C., and Thomas, F. O., "Plasma Actuators for Separation Control of Low Pressure Turbine Blades," *41st AIAA Aerospace Sciences Meeting and Exhibit*, AIAA, Ren, NV, Jan. 2003.
- <sup>13</sup>Matlis, E. H., *Controlled experiments on instabilities and transition to turbulence on a sharp cone at Mach 3.5*, Ph.D. thesis, University of Notre Dame, Indiana, 2004.
- <sup>14</sup>Orlov, D., Corke, T., and Haddad, O., "DNS Modeling of Plasma Array Flow Actuators," *Bulletin of the American Society Division of Fluid Dynamics*, Vol. 48, 2003.
- <sup>15</sup>Hall, K. D., Jumper, E. J., and Corke, T. C., "Potential Flow Model of a Plasma Actuator as a Lift Enhancement Device," *43rd AIAA Aerospace Sciences Meeting and Exhibit*, AIAA, Ren, NV, Jan. 2005.
- <sup>16</sup>Roy, S. and Gaitonde, D. V., "Modeling Surface Discharge Effects of Atmospheric RF on Gas Flow Control," *43rd AIAA Aerospace Sciences Meeting and Exhibit*, AIAA, Ren, NV, Jan. 2005.

<sup>17</sup>Suzen, Y. B., Huang, P. G., and Jacob, J. D., "Numerical Simulations of Plasma Based Flow Control Applications," *35th Fluid Dynamics Conference and Exhibit*, AIAA, Toronto, Ontario, June 2005.

<sup>18</sup>Assel, T. W., *Computational Study of Flow Over Elliptic Airfoils for Rotor/Wing Unmanned Aerial Vehicle Applications*, Master's thesis, University of Missouri-Rolla, Rolla, MO, 2007.

<sup>19</sup>Norton, K. E., *A Computational Study of the Flow Fields around Supersonic Airfoils and Subsonic Speeds*, Published by the author, 2006.

<sup>20</sup>Buning, P. G., Jespersen, D. C., Pulliam, T. H., Klopfer, G. H., Chan, W. M., Slotnick, S. E., and Renze, K. J., *OVERFLOW User's Manual : Version 1.8aa*, NASA, 2003.

<sup>21</sup>Enloe, C. L., McLaughlin, T. E., VanDyken, R. D., Kachner, K. D., Jumper, E. J., Corke, T. C., Post, M., and Haddad, O., "Mechanisms and Responses of a Single Dielectric Barrier Plasma Actuator: Geometric Effects," *AIAA Journal*, Vol. 42, No. 3, 2004, pp. 595-604.